Hindawi
Mathematical Problems in Engineering
Volume 2021, Article ID 1734542, 12 pages
https://doi.org/10.1155/2021/1734542

Research Article

Analysis of the Synthetic Electric Field of an UHVDC Transmission Tower in a High-Altitude Area

Hui Qu [1,2] **and Hechong Chen** [1]

[1]*Department of Electrical and Engineering, Wuhan University, Wuhan 430072, China*
[2]*State Grid Corporation of China, Beijing 100031, China*

Correspondence should be addressed to Hechong Chen; 2019102070026@whu.edu.cn

Received 12 August 2020; Revised 28 September 2020; Accepted 20 October 2020; Published 8 February 2021

Academic Editor: Michele Guida

The synthetic electric field of an ultrahigh voltage direct current (UHVDC) transmission tower in a high-altitude area is complex, which makes it difficult to protect the tower operators. Therefore, it is necessary to study the synthetic electric field. Firstly, this study establishes a mathematical model of the ion flow field and determines the solution process. Secondly, the relationship between the synthesis field of the transmission line and the ion mobility, wind speed, and the number of wire splits is analyzed using finite element simulations. Five typical operation positions are then selected for the simulation calculation of the composite field. Finally, the field measurement of the composite field is carried out, and the measurement results are compared with the simulation results. The accuracy of the simulation and theoretical analysis is verified by comparative analysis.

1. Introduction

At present, most of China's load centers are concentrated in developed provinces in the southeast, while energy centers are located in the east. One of the methods to solve this problem is to develop UHVDC transmission, which has the advantages of long distance, large transmission capacity, and low costs and losses compared with ultrahigh voltage alternating current (UHVAC) [1, 2]. In addition, with the continuous improvement of the national economic requirements for power supply reliability, the demand for live working on UHVDC transmission is increasing.

In the process of live working, the safety protection of the operator cannot be ignored. Through the efforts of experts and scholars, there are now standards and technologies in the safety protection measures of 110–1000 kV AC transmission lines [3–5]. Many studies on the effect of AC electric fields on human health have been carried out. Based on research results and the relevant standards of China, the maximum AC field intensity that live working operators on AC lines are exposed to should not be larger than 240 kV/m. For operators in shielding clothes, the maximum intensity should not be larger than 15 kV/m [6, 7]. Regarding the effect of the synthetic electric field on the human body in live work, relevant studies have reported that, under the same electric field value, the DC effect is smaller than the AC effect [8]. Since ±800 kV is the highest voltage level of a DC line, the synthetic field intensity combined by the space ion electric and electrostatic fields near the UHVDC transmission tower is more complicated than those of AC lines [9].

The entry of operators changes the distribution of synthetic electric and ion flow fields, thus making the analysis and calculation of body surface electric fields more difficult. Meanwhile, the high altitudes of the towers also affect the distribution of the ion flow field. Currently, there is no relevant research regarding these issues, and direct field measurements are also difficult to carry out. Therefore, under the conditions of high altitude, the question of whether the original safety protection tools and technical parameters for live working on 1000 kV UHVAC will continue to be used for live working on UHVDC of ±800 kV remains unanswered and requires further research. The

above problems seriously affect the personal safety of the operators during live working.

Based on the above research status, it is necessary to study the synthetic electric fields of UHVDC transmission towers in high-altitude areas. This study first establishes a mathematical model of the ion flow field and then analyzes its solution process. We also develop human body and transmission line models and analyze the influence of ion mobility, wind speed, and split wire on the composite field. The synthetic electric field of five typical working positions is then calculated using simulations. Finally, the field measurement of the synthetic electric field is carried out to verify the correctness of the simulation analysis.

2. Influence of Ion Flow Field on Distribution of Regional Electric Field

2.1. Mathematical Model of Ion Flow Field. Based on the physical characteristics of the ion flow field, an appropriate mathematical model is established and results that meet engineering accuracy requirements can be obtained through calculation and analysis. The solution of the UHVDC ion flow field is a boundary value problem under fixed boundary conditions and its governing equations are as follows:

$$\begin{aligned}
\nabla^2\varphi(t) &= -\frac{(\rho^+ - \rho^-)}{\varepsilon_0},\\
\mathbf{j}^+(t) &= \rho^+\left(k^+\mathbf{E}(t) + \mathbf{W}(t)\right),\\
\mathbf{j}^-(t) &= \rho^-\left(-k^-\mathbf{E}(t) + \mathbf{W}(t)\right),\\
\frac{\partial\rho^+(t)}{\partial t} + \nabla\cdot\mathbf{j}^+(t) &= -\left(R_{ion}/e\right)\rho^+(t)\rho^-(t),\\
\frac{\partial\rho^-(t)}{\partial t} + \nabla\cdot\mathbf{j}^-(t) &= -\left(R_{ion}/e\right)\rho^+(t)\rho^-(t),\\
\mathbf{E} &= -\nabla\varphi,
\end{aligned} \tag{1}$$

where $\mathbf{E}$ is the electric field strength (V/m); $\mathbf{j}^+$ and $\mathbf{j}^-$ are the positive and negative ion flow density (A/m^2), respectively; ρ^+ and ρ^- are the space positive and negative charge density (C/m^3), respectively; ε_0 is the dielectric constant of air (8.85×10^{-12} F/m); and k^+ and k^- are the mobility of positive and negative ions (m^2/(V·s)), respectively, which can be considered as the speed of the ions under the electric field, i.e., the ratio that the speed of ion movement to the electric field. Considering the approximate conditions, k is a constant, φ is the potential (V), and R_{ion} is the ion recombination coefficient.

For unipolar wires, there is no recombination of positive and negative ions in space, so the governing equation can be transformed as follows:

$$-\nabla\cdot(\nabla\varphi) = \frac{\rho}{\varepsilon_0}, \tag{2}$$

$$\nabla\cdot(\rho\nabla\varphi) = 0. \tag{3}$$

The solution variable of Equation (2) is potential φ. Equation (3) uses either φ as the solution variable or charge density ρ as the solution variable. Traditional methods mostly use ρ as the variable to solve the current continuity equation (Poisson). The process of solving the potential of the equation is positive, and the equation for solving the charge density through the current continuity equation is an inverse process. Each iteration step carries out two forward and reverse processes until convergence.

2.2. Solution Steps of Ionic Flow Field. In this study, the finite element method is used to calculate the ion flow field of an UHVDC transmission tower. This method discards the Deutsch assumption and uses an iterative method to solve the Poisson and current continuity equations to obtain the spatial electric field and ion flow distribution. According to the Kaptzov assumption, the surface field strength of the transmission line is maintained near the halo field strength. If the field strength on the surface is stronger than the halo field strength, a space charge emits and the amount of space charge generated can be considered as the sum of the charges generated at each node on the metal surface.

First, we set the initial value of the charge concentration of the halo boundary and calculate the electric field distribution in the steady state. We then take the maximum electric field value of the halo boundary and compare it with the halo field strength in air. If it is greater than the set criterion, the wire boundary corrects the charge concentration and continues the calculation. If it is less than the set criterion, then the calculation is completed and the charge density of the halo surface is obtained under the steady state. The convergence criterion used in the calculation of the steady state of the ion flow field of the DC transmission line is as follows:

$$\begin{aligned}
\frac{\left|E_{\max} - E_0\right|}{E_0} &= \delta_E < 1\%,\\
\frac{\left|\rho_i(n) - \rho_i(n-1)\right|}{\left|\rho_i(n-1)\right|} &= \delta_\rho < 1\%,
\end{aligned} \tag{4}$$

where $E_{\max}$ is the maximum electric field strength on the surface of the wire; E_0 is the halo field strength of the wire; $\rho_i(n)$ and $\rho_i(n-1)$ are the charge density at the space node i at n and $n-1$ iterations, respectively; and δ_E and δ_ρ are the relative deviations of the electric field intensity on the surface of the wire and the charge density of the space node, respectively.

If the calculated electric field intensity on the surface of the wire and the charge density of each node in the space cannot meet the convergence criterion simultaneously, the charge density on the surface of the wire needs correcting. This study proposes an iterative correction formula based on the Newton–Raphson method as follows:

$$\rho_i(n) = \rho_i(n-1) + \triangle\rho_i = \rho_i(n-1) - (\rho_i(n-1) - \rho_i(n-2))\left(\frac{E_0 - E_{\max n-1}}{E_{\max n-2} - E_{\max n-1}}\right), \tag{5}$$

where $\rho_i(n)$ and $\rho_i(n-1)$ are the charge density at node i of the wire surface at n and $n-1$ iterations, respectively, and μ is the correction factor, which is taken as two here.

In this work, a joint solution method based on MATLAB and COMSOL is used to calculate the ion flow field. Figure 1 shows the specific solution process.

3. Test and Calculation Model

3.1. Human Body Model. In order to calculate the electric field intensity on the body surface of live working operators, in the human body model, the electrical parameters mainly considered are the conductivity and relative dielectric constant. According to the research results, the relative dielectric constant of human living tissue at a frequency of 60 Hz is $\sim 1\times10^5$–2×10^6 [10]. This study assumes that the human body is a homogeneous medium. For the size of each human tissue, reference to the recommended value in *Human Dimensions of Chinese Adults* (GB10000-1988) [11–13] is taken. Therefore, the human body parameters are set as shown in Table 1.

3.2. ±800 kV UHVDC Transmission Line Model. This study takes the Yunnan-Guangdong ±800 kV UHVDC transmission tower as an example and simplifies the DC transmission line to a two-dimensional model for the analysis. The Yunnan-Guangdong ±800 k UHVDC transmission project adopts a single-circuit bipolar operation mode. The line parameters used in the calculation are a 6 × LGJ-630/45-type conductor, a subconductor diameter of $d = 33.6$ mm, a split spacing of $dc = 450$ mm, a conductor height to ground of $H = 18$ m, and a pole spacing of $D = 22$ m. The structure is shown in Figure 2.

In order to suppress corona discharge, UHVDC transmission lines mostly use split conductors to increase the radius of the conductors equivalently. The number of splits of the conductors increases as the voltage level increases. ±800 kV DC transmission lines in China use six-split conductors, while ±1100 kV DC transmission lines use eight split conductors. The model is usually simplified by splitting the wire into a single wire, as shown in Figure 3.

The equivalent radius of a single wire is calculated as follows:

$$R_{\text{eq}} = R\sqrt[n]{\frac{nr}{R}}, \tag{6}$$

where R_{eq} is the radius of a single wire equivalent to the split wire (cm), R is the radius of the circle passing through the center of each subwire of the split wire (cm), n is the number of splits of the wire, and r is the radius of the split wire (cm).

Considering the entire operating route of a live working operator from climbing the ladder to riding the suspended platform to entering the equipotential point, five typical positions representing different working conditions during the live working process are selected to measure and calculate the synthetic electric field intensity. Figure 4 shows the five typical positions. Position 1 is the tower body parallel to the conductor, position 2 is the cross arm perpendicular to the conductor, position 3 is 3 m away from the conductor, and positions 4 and 5 are both in the conductor, with position 5 3 m perpendicular to the plane.

4. Simulation of Synthetic Electric Field in High-Altitude Area

4.1. Convection and Electric Field Migration. When simultaneously considering convective transfer and electric field migration, the transient control equation of the dilute substance transfer module is

$$\begin{cases} \dfrac{\partial\rho}{\partial t} + \nabla\cdot(-D\nabla\rho - zuF\rho\nabla V) + w\cdot\nabla\rho = R, \\ \\ J = -D\nabla\rho - zuF\rho\nabla V, \end{cases} \tag{7}$$

where z represents the charge number of the tracer, F is the Faraday constant (96485 C/mol), and u represents the mobility (s·mol/kg).

Its structure is similar to the abovementioned current continuity equation and the meaning of each parameter is the same. However, since the electric field transfer characteristics of electric charges are not taken into consideration, it needs to be converted. Taking positive ion as an example, we can obtain Equation (1) as

$$\frac{\partial\rho^+(t)}{\partial t} + \nabla\cdot\left(\rho^+\left(-k^+\nabla\varphi + w - \frac{D^+\nabla\rho^+}{\rho^+}\right)\right) = -\left(\frac{R_{\text{ion}}}{e}\right)\rho^+(t)\rho^-(t). \tag{8}$$

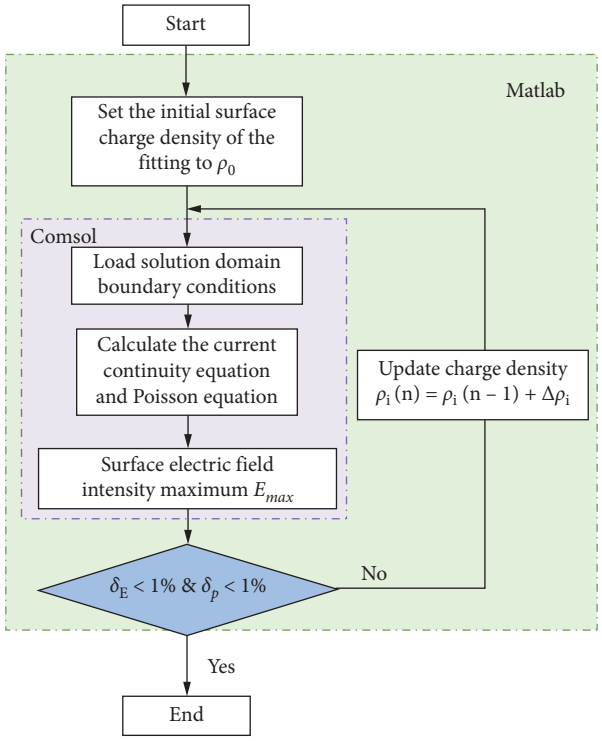

Figure 1: Solution process.

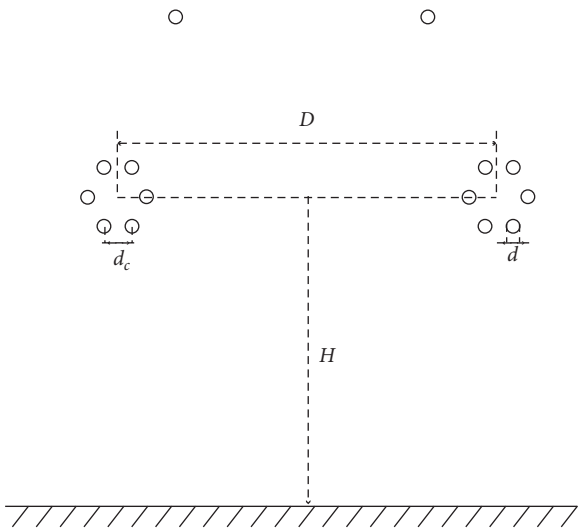

Figure 2: Simplified structure of the ±800 kV single-circuit bipolar DC transmission line.

Since $k+$, w, and $D+$ are constants, we can simplify Equation (8) to obtain

$$\frac{\partial \rho^+(t)}{\partial t} + \nabla \cdot \left(-D^+ \nabla \rho^+ - k^+ \rho^+ \nabla \varphi + \rho^+ w\right) = -\left(\frac{R_{\text{ion}}}{e}\right)\rho^+(t)\rho^-(t). \tag{9}$$

By comparing Equations (7) and (9), we can obtain the tracer charge number $z = 1$, and by letting $u = k/F$, the ion mobility can be determined. For the transmission line model shown in Figure 2, since the diffusion coefficient of the ions is relatively small, the effect of diffusion on the results can be ignored, so $D = 0$. According to Equation (9), we can

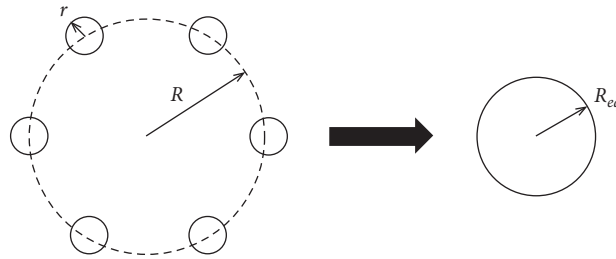

Figure 3: Six-split wire and its equivalent model.

Table 1: Human body parameters used in model.

Body part	Conductivity (S/m)	Relative dielectric constant	Shape (cm)
Head	0.1	10^5	Sphere: $r = 10$
Neck	0.1	10^5	Cylinder: $r = 8$, $h = 7$
Waist	0.1	10^5	Cylinder: $r = 16$, $h = 65$
Leg	0.1	10^5	Cylinder: $r = 10$, $h = 80$

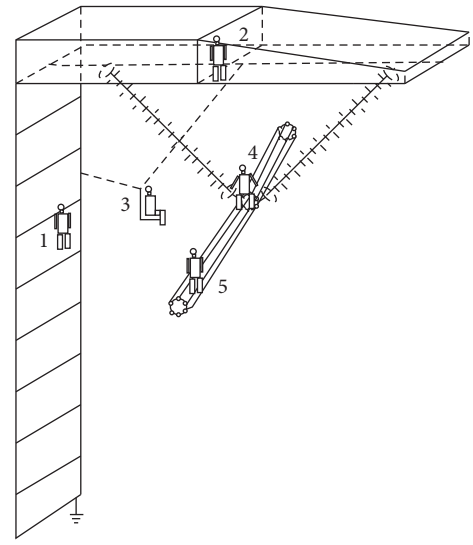

Figure 4: Typical positions of live working.

complete the setting of the COMSOL parameters. First, we iteratively obtain the charge density when the surface of the transmission line is haloed based on the charge density solution process shown in Figure 1. Figure 5 shows the results of the segmentation.

Finally, considering the convection and electric field migration, the distribution of the electric field strength and charge density in the field under a halo field strength of $E0 = 4.8$ kV/cm is shown in Figure 6.

From the above calculation results, when both convection and electric field migration are considered, the maximum charge concentration in the calculated charge density in the steady-state field is $3.4 \times 10{-}8$ C/m3. Considering convection and electric field migration, the calculated electric field strength and charge density distribution in the field under a halo field strength of $E0 = 4.2$ kV/cm are shown in Figure 7.

From the above calculation results, when convection and electric field migration are considered simultaneously, the maximum charge concentration in the calculated field in the steady state of the charge density is $6.19 \times 10{-}8$ C/m^3. According to Figures 6 and 7, the higher the halo field strength, the lower the charge density around the transmission line. In consideration of convection and electric field migration, Figure 8 shows the combined ground electric field under different halo field strengths. The results in Figure 8 are also consistent with the actual situation. The lower the halo field strength, the greater the ground synthetic electric field strength.

4.2. Effect of Wind Speed. Wind speed has a direct effect on the diffusion of space charge. Taking the above model as an example, the synthetic electric field is simulated at wind

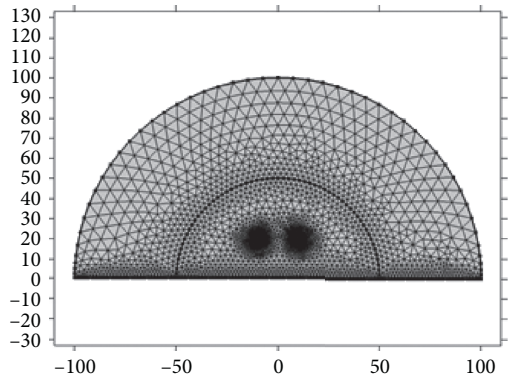

Figure 5: Schematic diagram of field segmentation.

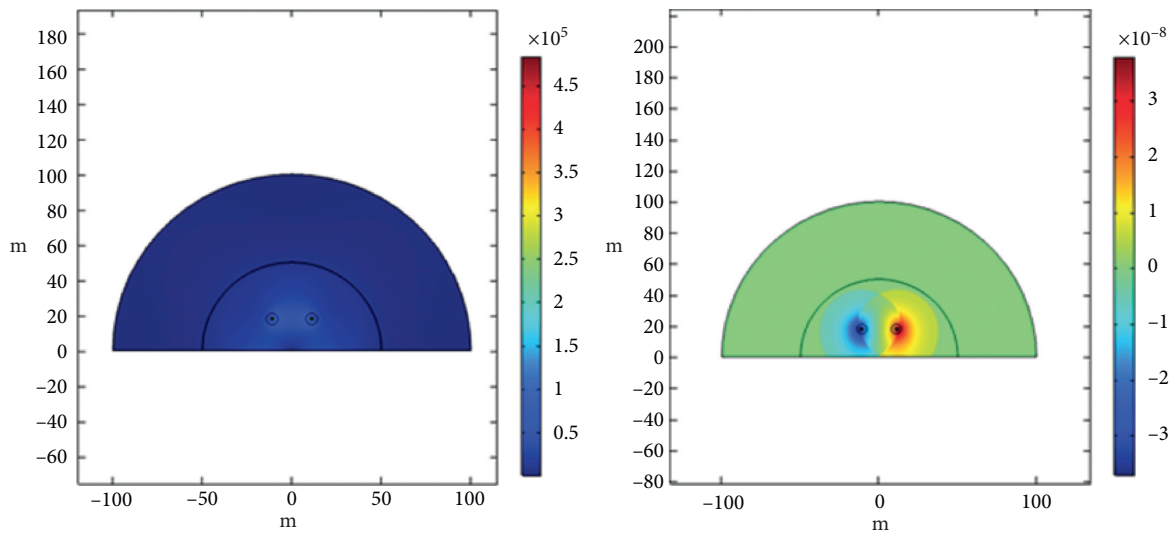

Figure 6: Results for a halo field strength of 4.8 kV/cm: (a) space electric field strength (V/m); (b) space electric field density (C/m^3).

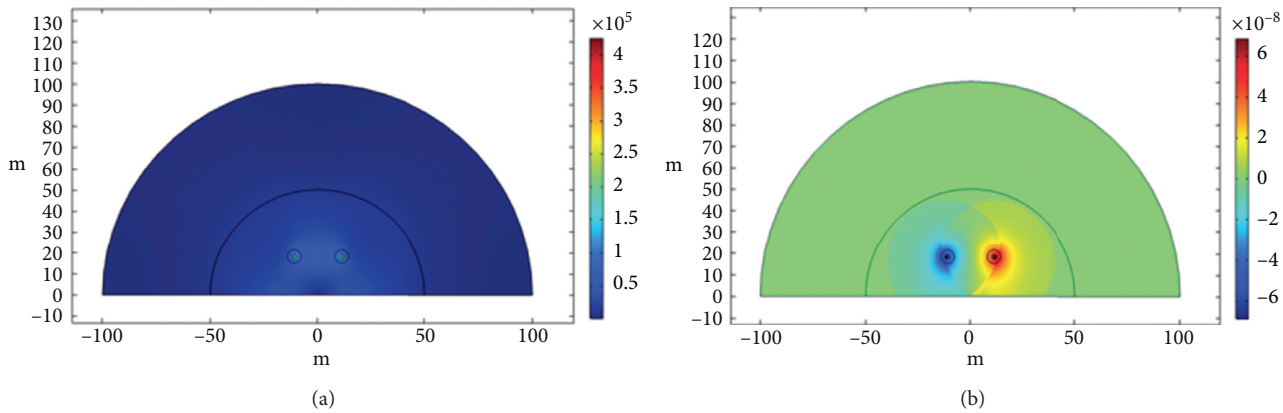

Figure 7: Results for a halo field strength of 4.2 kV/cm: (a) space electric field strength (V/m); (b) space electric field density (C/m^3).

speeds of 2 and 10 m/s, with the results of the electric field strength and charge density distribution under these wind speeds, as shown in Figures 9 and 10.

It can be seen from the above calculation results that when the wind speed increases from 2 to 10 m/s, the charge diffusion range increases significantly with the wind

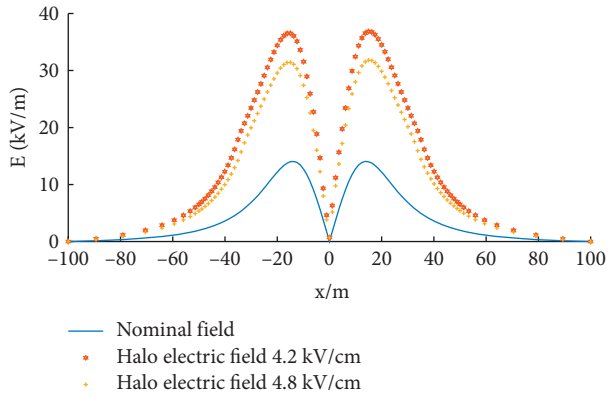

Figure 8: Electric field strength of ground under different halo field strengths.

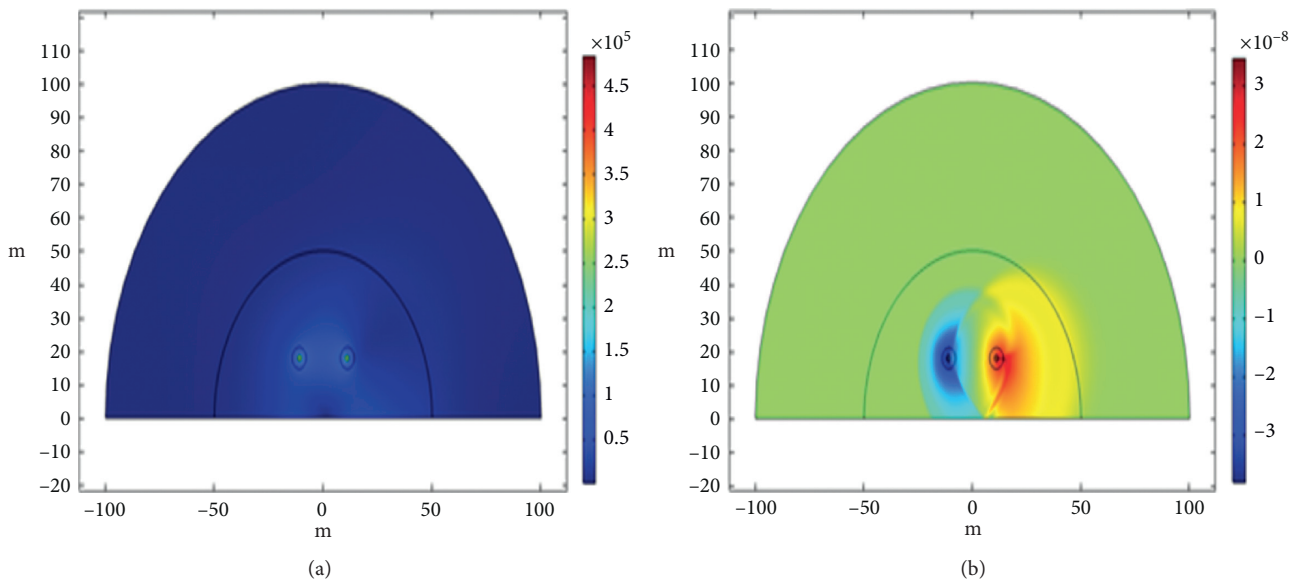

Figure 9: Results for a wind speed of 2 m/s: (a) space electric field strength (V/m); (b) space electric field density (C/m^3).

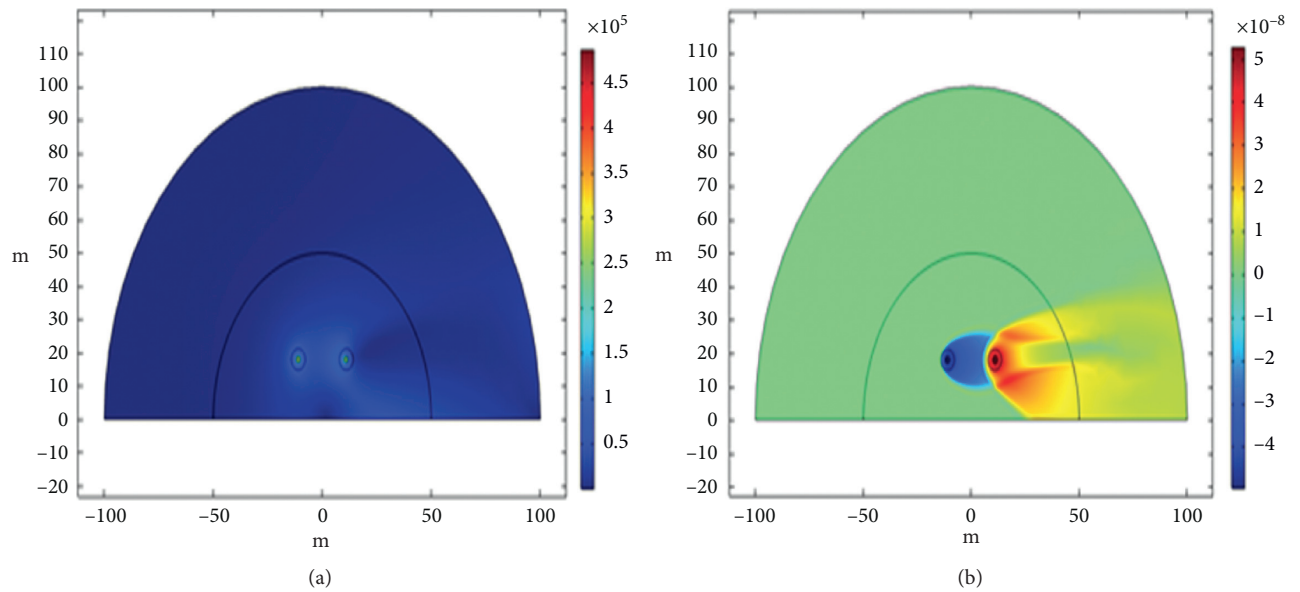

Figure 10: Results for a wind speed of 10 m/s: (a) space electric field strength (V/m); (b) space electric field density (C/m^3).

direction. Therefore, when simulating a high wind speed environment, the influence of wind speed must be fully considered. According to Figures 9 and 10, the electric field strength near the wire is maintained near the halo field strength, which satisfies the Kaptzov assumption. Considering the wind speed, the halo field strength is 4.8 kV/m and the ground synthetic electric field under different wind speeds is shown in Figure 11.

It can be observed from Figure 11 that the solution calculated in this work is close to the solution obtained in the literature and basically maintains a consistent distribution trend. Simultaneously, it can be found that, due to the effect of wind speed, the maximum value of the ground synthetic field strength is not directly under the transmission line conductor but is offset by ~4–5 m. The simulation result is the same as the actual measured value. The results of the comparison of the ground synthetic and nominal electric fields with the measured values of this method are shown in Table 2.

The ion flow field calculated in this study is significantly improved in calculation accuracy compared to the nominal electric field calculated by traditional methods, and the maximum deviation of the nominal electric field gradually increases as it moves away from the maximum electric field point, which is much larger than the electric field deviation calculated by the method. The ground synthetic electric field calculated by this method is 2.4 times the nominal electric field, and the deviation from the actual maximum measured value is only 1.02%. The wind speed in this work is loaded by the crosswind speed, but the direction of the wind has a certain transient change during the actual measurement. Therefore, the calculation results of this method have only a minor deviation from the actual measured values.

4.3. Effects of Split Wires. In the calculation of the ion flow field of a DC transmission line, if the research focus is on the ion flow density and electric field characteristics of the area near the wire, it is important to consider the area near the split wire, so the split wire cannot be equivalent to a single wire as a way to simplify the model. Simultaneously, the charge in the air also has diffusion characteristics, so the drift-diffusion equation is introduced. The diffusion coefficient and mobility are expressed by the Einstein relationship as

$$D^{+} = \frac{k^{+} k_b T}{e}, \qquad D^{-} = \frac{k^{-} k_b T}{e}. \tag{10}$$

The line parameters used in the calculation are 6 × LGJ-630/45-type conductors, a subconductor diameter of $d = 33.6$ mm, a split spacing of dc = 450 mm, a conductor height to ground of $H = 18$ m, and a pole spacing of $D = 22$ m. The height of the lightning conductor to the ground is 33 m. The results of the split are shown in Figure 12. The final results of the electric potential and field intensity distribution are shown in Figure 13.

The advantage of the finite element method is not only that it can solve the ion flow field problem of complex structural models but also can deal with the influence of wind speed on the spatial ion flow field. For the above-mentioned bipolar DC test line with a conductor of ±800 kV, we consider the effect of wind speed, calculate the synthetic electric field near the ground, and analyze the relationship between the synthetic electric field strength near the ground and the wind speed. The wind speed in the positive direction of x is applied and is 0 and 2 m/s, respectively. The results of the ground synthetic electric field strength calculation are shown in Figure 14.

Research shows that the DC synthetic field strength is greatly affected by the wind speed. The synthetic field strength on the upwind side decreases with increasing wind speed, and the synthetic field strength on the downwind side increases with increasing wind speed. The research results show that the maximum point of the ground synthetic electric field is shifted in the presence of wind. Moreover, when calculating the ground synthetic electric field, the results of calculating the equivalent single and split wires are basically the same.

4.4. Synthetic Electric Field Simulation of Typical Working Positions. Based on the above analysis, the synthetic electric field simulation of the typical operating positions was carried out under the conditions of a wind speed of 2 m/s, positive and negative ion mobilities of 1.5 and 1.7 × 10–4 m2/(V·s), respectively, and six-split conductors of the transmission line.

The synthetic electric field intensity combined by the space charge electric field and electrostatic field near the ±800 kV UHVDC transmission line and the current characteristics during potential transfer are more complicated than those of an AC line. In this study, the simulation calculation of the synthetic electric field for five typical working positions is carried out by the finite element method. Through simulations, the characteristics chart of the electric field intensity distribution around the ±800 kV UHVDC line after considering the tower is obtained. The calculation results of the synthetic electric field at the two positions representing the typical working conditions on the tower are shown in Table 3.

Based on the characteristics of the electric field intensity distribution around the line, the electric field intensity on the operator's body surface at three typical positions representing different working conditions in the air is obtained. The calculation results of the synthetic electric field at different positions are shown in Table 4.

5. Field Measurements of Synthetic Electric Fields

5.1. Typical Field Measurements of Synthetic Electric Fields. In the measurement process, the operator wears shielding clothes to climb the tower and arrives at each typical position on the tower to measure the synthetic electric field intensity. The field measurement is shown in Figure 15. When

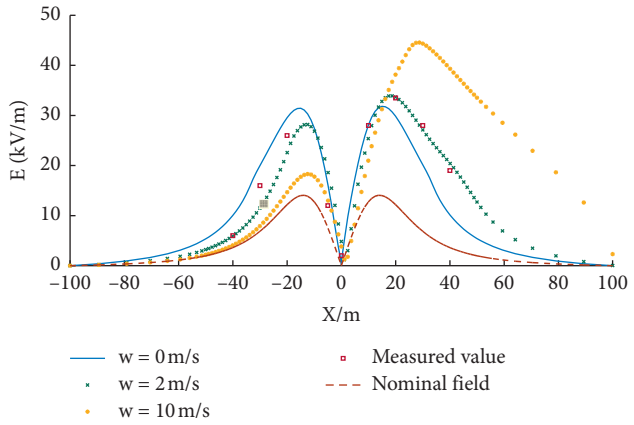

Figure 11: Results for ground synthetic electric field under different wind speeds.

Table 2: Comparison between this study and the deviation of the nominal electric field and the measured value.

	Maximum electric field strength	Maximum electric field deviation (%)	Maximum deviation (%)
This article method	33.94	1.02	21.6
Nominal electric field	14.16	58.8	81.1

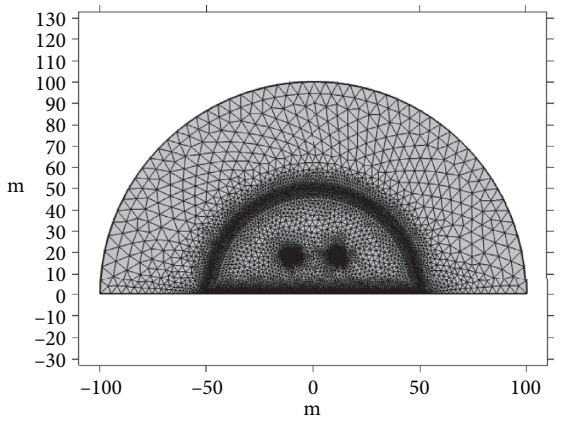

Figure 12: Schematic diagram of two-dimensional model field segmentation.

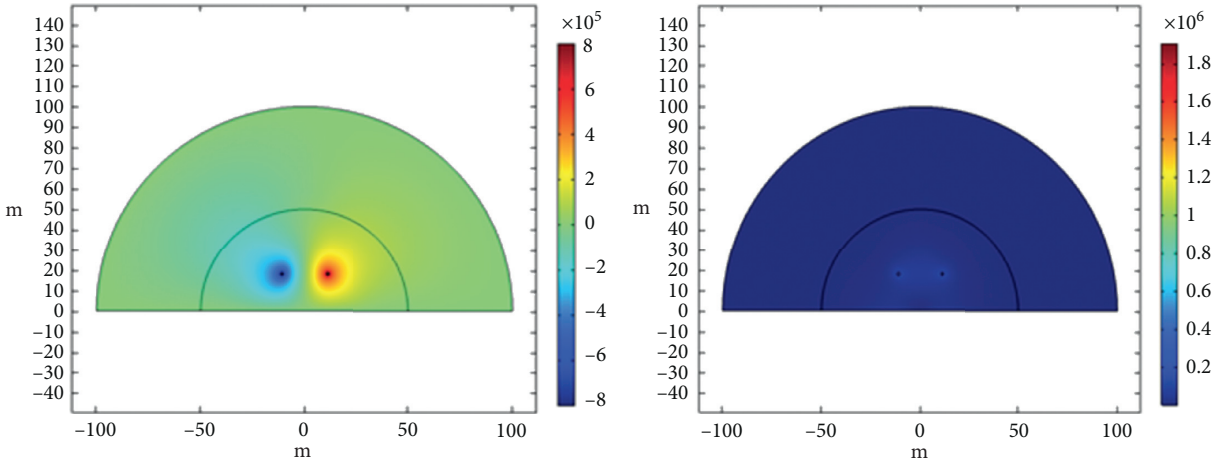

Figure 13: ±800 kV UHVDC line result diagram: (a) space electric field strength; (b) space charge density.

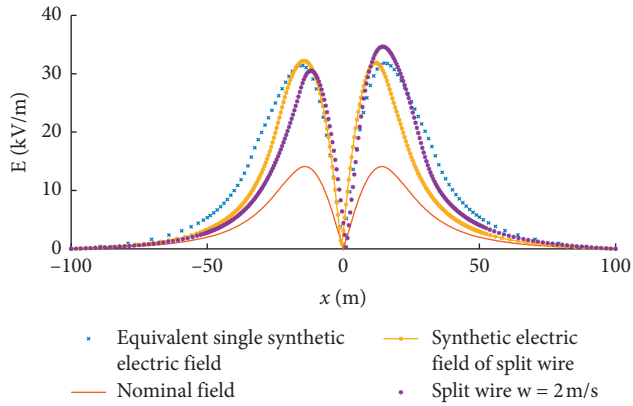

Figure 14: Ground synthetic electric field result graph.

Table 3: Calculation results of synthetic *l* electric field around the tower.

Measuring position		Simulation result (kV/m)
Position 1	Inside the tower	9.1
	Outside the tower	54.1
Position 2	Inside the tower	13.6
	Outside the tower	27.3

Table 4: Calculation results of synthetic electric field on human body surface.

Measuring position		Simulation result (kV/m)
Position 3	Top of the head	162.4
	Chest	44.6
	Hand	52.9
	Toes	184.2
Position 4	Top of the head	1710
	Chest	24.8
	Hand	1650
	Foot	406
Position 5	Top of the head	1690
	Chest	24.5
	Hand	1640
	Foot	661

measuring the electric field intensity on the human body surface, the environmental parameters of the test site are shown in Table 5.

The field measurement results of the synthetic electric field are shown in Table 6 and are compared with the simulation results.

By comparing the simulation and field measurement results, it can be seen that the calculated and measured values at the positions with lower electric field intensity are in good agreement with each other, while the calculated and measured values at the positions with higher electric field intensity are greatly different, with the calculated values obviously greater than the measured values. This is because the use of instruments with metal parts in the field measurement makes the measured values smaller than the true values, while in the simulation calculation, the influence of the corona phenomenon on the electrostatic field is not considered. Therefore, the calculated values are larger than the true values. Meanwhile, the distortion of the electric field caused by the corona phenomenon is not obvious in the place with a small electric field intensity but more remarkable in the place with a large electric field intensity.

Through the above analysis, it can be concluded that the true value will be between the calculated and measured values so that the true value can be effectively estimated.

5.2. Analysis of Synthetic Electric Field Characteristics. Through the simulations and analysis of the field measurement results, the characteristics of the electric field intensity distribution on the body surface of live working operators of the ±800 KV UHVDC line were determined:

Figure 15: Field measurement of electric field.

Table 5: Environmental parameters of test site.

Environmental indicators	Numerical value
Altitude	2100m
Temperature	23.6°C
Relative humidity	49.5%
Air pressure	79.3 kPa
Wind speed	2m/s

Table 6: Field measurement results of synthetic electric field.

Measuring position		Simulation result (kV/m)	Measurement result (kV/m)
Position 1	Inside the tower	9.1	4.0
	Outside the tower	54.1	26.0
Position 2	Inside the tower	13.6	6.0
	Outside the tower	27.3	48.4
Position 3	Top of the head	162.4	132.0
	Chest	44.6	96.2
	Hand	52.9	241.5
	Toes	184.2	150.0
Position 4	Top of the head	1710	404.2
	Chest	24.8	39.1
	Hand	1650	529.0
	Foot	406	145.3
Position 5	Top of the head	1690	400.6
	Chest	24.5	37.7
	Hand	1640	560.5
	Foot	661	250.4

(1) When the operator is at ground potential, the electric field intensity on his or her body surface is smaller than the warning value of 240 kV/m.

(2) After the operator enters the equipotential position and is at the equipotential position, the electric field intensity on some body parts is greater than 500 kV/m, thereby exceeding the warning value. Hence, protection should be focused on these parts.

By comparing the above field measurement data for the electric field intensity on the body surface of equipotential operators (at positions 4 and 5 with previous data of operators working on UHVAC transmission lines), it is found that the electric field intensity on top of the head and at the hands of the equipotential operators on the ±800 kV UHVDC lines is less than 650 kV/m (inclusive) and that of equipotential operators on 1000 kV UHVAC lines is ~1800–2500 kV/m. It is also found through comparison of the data at other positions that the electric field intensity on the body surface of the equipotential operators on ±800 kV UHVDC lines is significantly smaller than that on the 1000 kV UHVAC lines.

6. Conclusion

(1) We use a new method of ion flow field calculation and show that the higher the halo field strength, the lower the charge density around the transmission

line. In consideration of convection and electric field migration, the lower the halo field strength, the greater the ground synthetic electric field strength.

(2) The synthetic field strength under the DC transmission line is greatly affected by wind speed. The synthetic field strength on the upwind side decreases with increasing wind speed, and the synthetic field strength on the downwind side increases with increasing wind speed. In the presence of wind, there is a shift in the maximum point of the ground synthetic electric field. Moreover, when calculating the ground synthetic electric field, the results of calculating the equivalent single and split wires are basically the same.

(3) The maximum value of the electric field intensity on the body surface of an operator at ground potential during live working on ±800 kV DC transmission lines is 50–60 kV/m. Protective measures should be taken in the process of entering the equipotential and at this time, the electric field intensity on the body surface of equipotential operator exceeds 240 kV/m.

Data Availability

The data used to support the findings of this study are available from the corresponding author upon request.

Conflicts of Interest

The authors declare that there are no conflicts of interest.

Acknowledgments

This work was supported by the National Natural Science Foundation of China project (Grant no. 51177111).

References

[1] W. Yu, Y. Xue, J. Luo, M. Ni, H. Tong, and T. Huang, "An UHV grid security and stability defense system: considering the risk of power system communication," *IEEE Transactions on Smart Grid*, vol. 7, no. 1, pp. 491–500, 2016.

[2] P. Maruvada, R. D. Dallaire, P. Heroux, and N. Rivest, "Long-term statistical study of the corona electric field and ion-current performance of a ±900-kV bipolar HVDC transmission line configuration," *IEEE Transactions on Power Apparatus and Systems*, vol. PAS-103, no. 1, pp. 76–83, 1984.

[3] Yi Hu, L. N. Wang, and G. W. Shao, "Live working ways for compact transmission lines and relevant safety protection," *Power System Technology*, vol. 23, no. 31, pp. 6–10, 2007.

[4] Y. Hu, K. Liu, T. Wu et al., "Key technology research and application of live working technology on EHV/UHV transmission lines," in *Proceedings of the International Conference On Power System Technology*, pp. 2299–2309, IEEE, Chengdu, China, October 2014.

[5] L. Kai, L. Wang, H. Yi et al., "Research of safety protection for live working on 1000kV AC ultra high voltage transmission line," *High Voltage Engineering*, vol. 36, no. 11, pp. 2668–2673, 2010.

[6] B. Xiao, L. Kai, C. Lei et al., "Investigation on insulating platform for live working on 1 000kV UHV substation," *High Voltage Apparatus*, vol. 321, no. 12, pp. 6–10, 2015.

[7] D. C. Huang, R. Jiang-Jun, and S. B. Liu, "Potential distribution along UHV AC transmission line composite insulator and electric field distribution on the surface of grading ring," *High Voltage Engineering*, vol. 36, no. 1, pp. 1442–1447, 2010.

[8] Y. Hu, J. X. Hu, K. Liu et al., "Field strength of body surface during the live working on the UHV AC and DC transmission lines," *High Voltage Engineering*, vol. 36, no. 1, pp. 13–18, 2010.

[9] M. G. Omber and G. B. Johnson, "HVDC field and ion effects research at project UHV: results of electric field and ion current measurements," *IEEE Transactions on Power Apparatus & Systems*, vol. 24, no. 1, pp. 3–9, 1982.

[10] C. C. Reddy and T. S. Ramu, "On the computation of electric field and temperature distribution in HVDC cable insulation," *IEEE Transactions on Dielectrics & Electrical Insulation*, vol. 1, pp. 1236–1244, 2006.

[11] Human Dimensions of Chinese Adults, GB10000-1988, CSBTS, 1987.

[12] Screen Clothes for Live Working, GB/T6568-2008, SAC, 2007.

[13] Y. Zhang, C. Bin, Qiu Zhonghua et al., "Study on the path of live operation of ± 800 kV UHV DC line into equipotential based on human body surface field strength," *High Voltage Technology*, vol. 45, no. 4, 2019.